energies

MDPI

Article

Hygrothermal Performance Evaluation of Internally Insulated Historic Stone Building in a Cold Climate

Andra Blumberga, Ritvars Freimanis, Edite Biseniece and Agris Kamenders *

Institute of Energy Systems and Environment, Riga Technical University, Azenes 12/1, LV-1048 Riga, Latvia; andra.blumberga@rtu.lv (A.B.); ritvars.freimanis@rtu.lv (R.F.); edite.biseniece@rtu.lv (E.B.)
* Correspondence: agris.kamenders@rtu.lv; Tel.: +371-2951-6506

Abstract: In most cases, internal insulation is the only solution to improve the energy efficiency of historic buildings. However, it is one of the most challenging and complex energy efficiency measures due to changes in boundary conditions and hygrothermal behavior of the wall, particularly in cold climates. This study presents the long-term monitoring of the hygrothermal performance of an internally insulated historic stone wall building. The study aimed to assess the hygrothermal behavior of the dolomite wall if mineral wool insulation is applied internally on the north-east wall in the rooms with and without high internal moisture load. The measurements included temperature, relative humidity, water content, and heat flux. Monitoring results are compared with 1D hygrothermal simulations and a building energy consumption simulation. The in situ measurement results and hygrothermal assessment shows energy consumption decreased by 55% with relative humidity under the insulation staying belove 60% for most of the time, with short periods of increase over 80%. Energy consumption simulation shows an energy saving potential of up to 72% in the case of proper energy management.

Keywords: energy efficiency; energy retrofit; historic building; internal insulation; DELPHIN; TRNSYS; dolomite stone; thermal performance; building energy simulation; building hygrothermal simulation

Citation: Blumberga, A.; Freimanis, R.; Biseniece, E.; Kamenders, A. Hygrothermal Performance Evaluation of Internally Insulated Historic Stone Building in a Cold Climate. *Energies* **2023**, *16*, 866. https://doi.org/10.3390/en16020866

Academic Editor: Abu-Siada Ahmed

Received: 5 December 2022
Revised: 8 January 2023
Accepted: 9 January 2023
Published: 12 January 2023

1. Introduction

The European Commission has set a target to reduce 40% of greenhouse gas emissions by 2030 [1]. It also aims to be climate neutral by 2050, in line with the objectives of the Paris Agreement [2]. The building sector is Europe's single largest energy consumer, accounting for 40% of EU energy consumption and 36% of greenhouse gas emissions [3]. Space heating takes a 67% share of the end-use in the residential sector [4].

A significant renovation of existing buildings, regardless of their size or retrofit of building elements, provides the opportunity to take a cost-effective measure to improve the energy performance of the existing building stock. According to the European Commission, the annual renovation rate of the building stock varies from 0.4 to 1.2% in the Member States. However, this rate will need to at least double if targets set by the European Commission are to be met [5]. Moreover, a life cycle cost analysis [6] shows that costs are higher for the demolition and rebuilding of older dwellings compared to retrofitting to the same energy standards without even considering the apparent increase in emissions associated with demolition and rebuilding [7,8].

More than 40% of European residential buildings were built before 1960 [9], and many of these buildings are considered to have cultural heritage value. These buildings were built when energy efficiency requirements were non-existing or non-demanding, and most of these buildings will still be actively used in 2050 [10]. The most significant challenges of the renovation of buildings occur in retrofitting heritage buildings where the facade cannot be modified as the building's unique architectural appearance, and integrity

needs to be maintained [11–13]. In addition, it is hard to evaluate the building's energy performance, as the technical documentation of old buildings often needs to provide adequate documentation of the present conditions or is not available at all [14]. For example, data from 2011 show that in Latvia, annual heating energy consumption in historical buildings (built before 1945) is estimated at approximately 31% of the total final heating energy consumed by residential and non-residential building sectors [15].

The most common approach to improve the buildings' thermal performance is installing external insulation on walls, window replacement, and insulation of basement ceilings and the building's roof [16–19]. Implemented simultaneously, these are by far the most efficient measures [20,21]. However, for buildings with historically valuable facades, only a few of these measures can be applied, such as insulation of the basement and roof, which alone do not produce the desired energy savings. In these cases, external insulation is not an option as it covers the historical heritage of the facade. The only other option is internal insulation of the walls, which allows reducing a building's operational energy and its associated negative impact on the environment [22,23].

Internal insulation, however, changes the hygrothermal conditions of the building envelope. This may negatively impact the hygrothermal performance of the building's wall [13,24,25]. Moisture control of the walls is different in modern buildings and historic buildings. Modern buildings protect external walls from impermeable membranes, wall cavities, and damp-proofing. In historic buildings, walls are built from locally sourced heterogeneous materials, using traditional craftsmen methods, controlling moisture by allowing the building fabric to wet and subsequently dry through materials and assemblies that both adsorb moisture and allow it to evaporate quickly [26]. If internal insulation is applied, the original wall remains on the structure's cold side, which reduces any potential drying of the wall. Hence, internal insulation may increase the risk of interstitial condensation, frost damage, decay of embedded wooden beams, and mold growth [25,27–33]. Moreover, internal insulation does not eliminate thermal bridges [23,34].

Water transport properties and anisotropy depend on a material's porosity, pore structure, textural characteristics, and mineralogy [35]. One of the stones used in historic buildings is dolomite rock or dolostone. It is a sedimentary carbonate rock with a high percentage of the mineral dolomite. These stones have been used as building materials for centuries because they are easy to work with, are easily accessible, and have a high aesthetic value at a relatively low cost [36]. Different studies have investigated the use of dolomite rock as a construction product in historic buildings, their decay, and conservation treatments [35,37–39]. Numerous papers report in situ heat transfer and moisture transport measurements in internally insulated masonry walls, both successful and unsuccessful examples. One study reports the flawless hygrothermal performance of an internally insulated 19th Century brick building in Prague that was insulated using hydrophilic mineral wool without a vapor barrier; during the 4-year in situ study, there was no interstitial water condensation [40]. Another study was carried out for internally insulated brick walls with different insulation materials (calcium silicate (CaSi), aerated concrete (AAC), polyurethane board with active capillary channels (IQ-T), and polyisocyanurate (PIR)); in the study, they found that IQ-T and PIR were performing similar regardless the capillary activity of IQ-T, both had high relative humidity (over 80%) under the insulation, CaSi and AAC showed a similar pattern of RH behind the insulation. CaSi maintained an Rh under 80%, while AAC exceeded 90%, but as mentioned by the authors, the hygrothermal performance of an insulated wall only partially depends on insulation material, properties, and thickness of the original wall, which also influences the performance and the built-in moisture [41]. Moreover, a holistic energy renovation (moisture safety and energy efficiency are balanced) approach has been studied, and 47% energy reduction was achieved in the case study building; in this study, one of the main conclusions was that a more detailed study over a longer period is necessary to decrease the uncertainty of results [31]. In a study about the rehabilitation of historical façade buildings, the full utility of AAC as internal insulation was confirmed, and the authors pointed out the important role of simulations

in predicting the long-term hygrothermal state of the internally insulated buildings [42]. One of the leading research institutes of the Technical University of Denmark performed hygrothermal measurement in four case-study buildings with different internal insulation materials, they concluded that vapor-open insulation systems overall performs better than vapor-tight systems, but they also concluded that other parameters, such as insulation thickness, surface treatment, and the external hygrothermal loads, have a high impact on the performance [43]. Moreover, our research institute has a previous experience in this field of study [44].

However, reviewing the research papers demonstrated a need for more research on hygrothermal performance and energy savings of internally insulated dolomite stone buildings.

This study aims to answer the following two research questions: (1) What is the impact of internally insulated natural stone buildings on the hygrothermal behavior of walls in a cold climate? (2) What energy savings can be reached by internal insulation of natural stone buildings in a cold climate? In comparison to existing research papers in our research, we monitored on-site indoor and outdoor climate, including solar radiation, and in addition to the relative humidity and temperature measurements in between the layers of internal insulation, we monitored volumetric moisture content of the external wall and performed mathematical simulations of the monitored building.

The paper starts with an introduction, followed by a description of the case study building, applied methodology, analysis of results, discussion, and finally, conclusions.

2. Case Study Building

2.1. Background Information

The case study building is a single-family home in the countryside in Sece parish, Aizkraukle county, Latvia. It was built in 1893 as a farmhouse. During the period after the second world war until the 21st century, the building was poorly maintained; the basement was used as a cattle shed which led to severe damage to the wooden beams and ground floor cover. In 1992, the building was denationalized, and the ownership of the building was retrieved by the family of the building's original owner.

The building has two floors with a total heated area of 339 m^2 and a volume of 870 m^3. The basement (floor area 68 m^2 and volume 130 m^3) occupies half of the building's floor area on the south-east façade and is not heated. The facade has a total area of 274 m^2, including windows and doors but excluding the basement part.

The external walls are constructed from locally sourced dolomite stone embedded in mortar. For basement walls, granite stones are used as well. Granite chips are also used to cover mortar joints between dolomite stones (Figure 1).

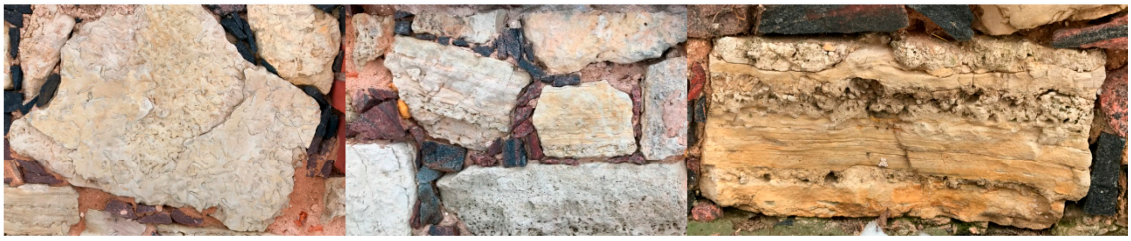

Figure 1. Structural patterns of dolomite stones in the external wall of the building.

The walls have a thickness of 0.60 m (ground floor and basement) and 0.45 m (1st floor). Brick columns are built in the corners and around the windows as a frame. The interior side of the external walls has an originally installed plaster layer. In 2006, after full-scale roof reconstruction, two dormers were added on the west and east sides of the house (see Figure 2).

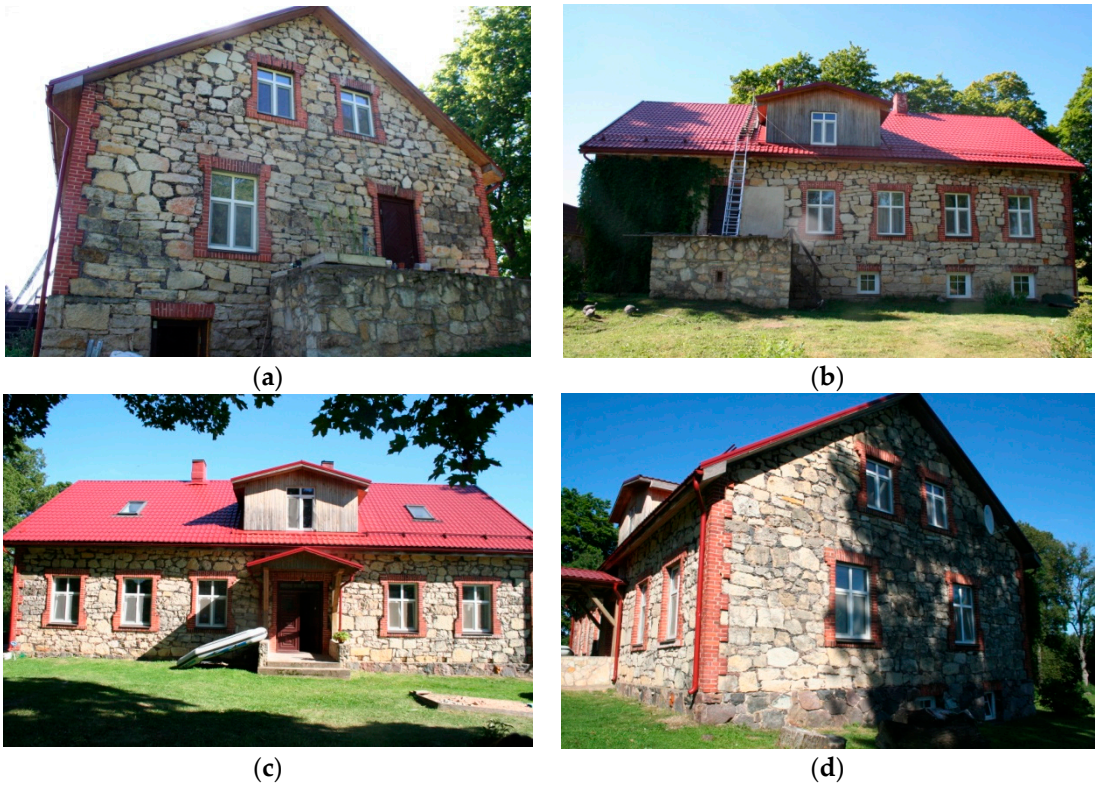

Figure 2. Facades of the case study building: (**a**) north-east, (**b**) south-east, (**c**) north-west, (**d**) south-west.

2.2. Energy Efficiency Measures

Two rounds of energy efficiency renovation were made. The main goal of both renovations was to decrease firewood consumption by decreasing heat loss through the building envelope. In 2006, the following measures were carried out:

- Internal insulation of the building walls on the ground and first floor with 0.15 m of mineral wool and installation of Ruberoid as a vapor barrier between the dolomite and insulation (moisture diffusion resistance equivalent of still air (Sd) = 15 m)
- Insulation of the basement ceiling with 0.25 m of expanded clay;
- Insulation of the roof with 0.30 m of mineral wool;
- Change of windows (U = 1.26 W/m^{2}K);
- Installation of wood boiler and water heating system with radiators;
- Installation of a hot water supply with a heat accumulation tank;
- Installment of cold water supply and sewage system.

Nine years later, based on the building residents' observations, the ground floor premises seemed colder, and firewood consumption had increased compared to the situation before the first round of the renovation. In 2015, the walls and floors of the ground floor rooms occupied all year were inspected (see Figure 3). The inspection revealed that the mineral wool was heavily inhabited by martens and rats, which had created a system of burrows within the walls. It was also discovered that in the bathroom located in the north corner of the building (see Figure 3, red line), the dolomite stone walls behind the mineral wool were covered with a black layer of mold. In 2015, the second round of renovation was carried out, and the old insulation was replaced with a new internal insulation system:

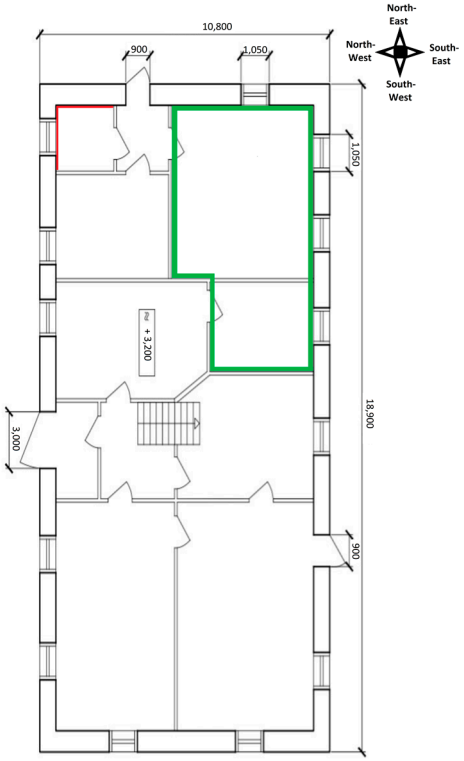

Figure 3. Inspected insulation on the ground floor in 2015: damaged floor and external wall insulation by martens (green) and a black layer of mold between the dolomite stone wall and mineral wool (red).

Insulation of the basement ceiling with expanded clay (0.25 m, $\lambda = 0.11$ W/mK) in the green part in Figure 3.

Mineral wool insulation (0.15 m in the rooms and 0.2 m in the bathroom, $\lambda = 0.04$ W/mK) in combination with an expanded clay layer (0.15 m thickness, 0.2 m from the ground) in both the green and red parts in Figure 3.

The vapor barrier was installed between mineral wool and plasterboard.

The cross-section of the living room's wall and the floor is presented in Figure 4.

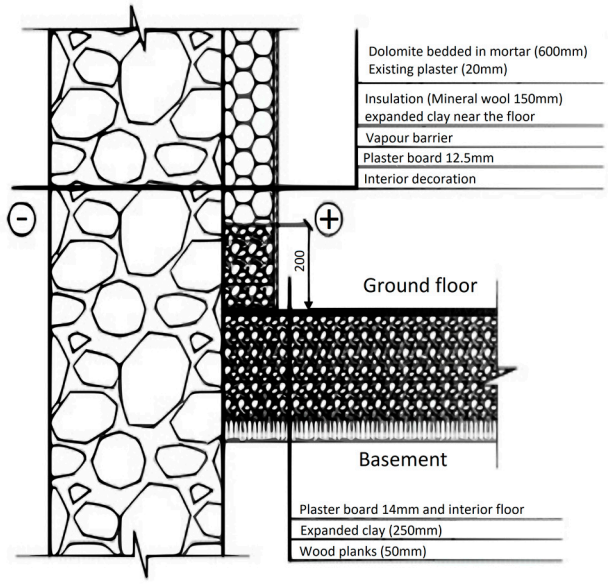

Figure 4. The cross-section of the living room's wall and floor construction after renovation in 2015.

After the renovation in 2015, external walls were divided into four types (see Figure 5).

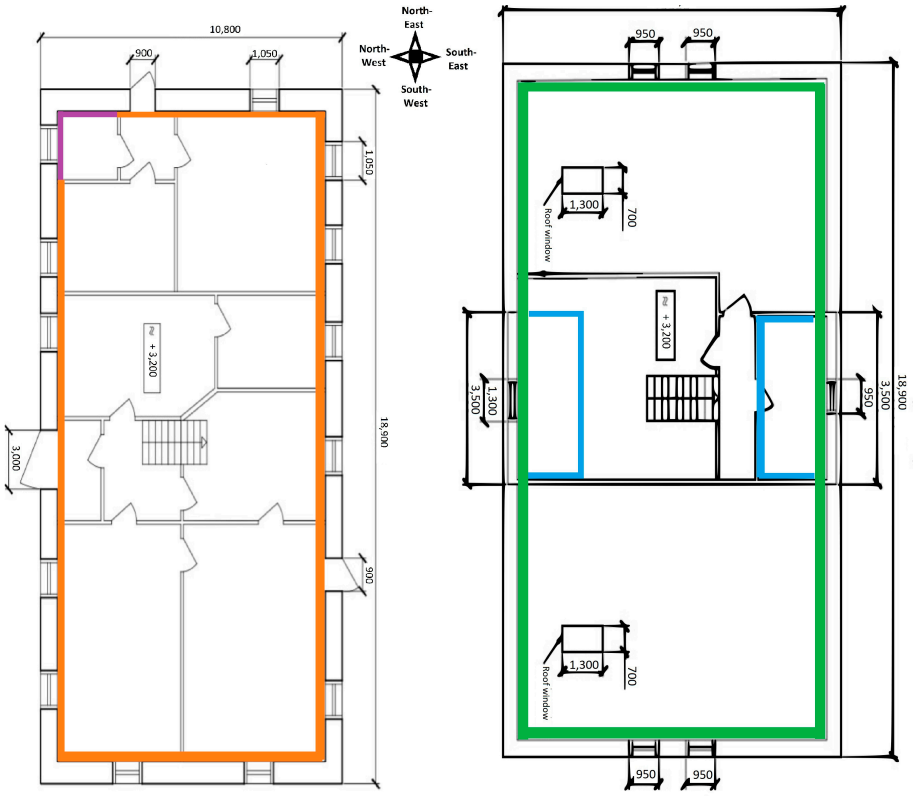

Figure 5. Location of four wall construction types in zones A2 after renovation in 2015, on the left 1st floor, on the right 2nd floor: type 1(purple), type 2 (orange), type 3 (green), and type 4 (blue).

Tables 1–4 contain detailed information about the different types of external walls.

Table 1. Facade construction after retrofit in 2015: Type 1.

Material	Thickness (mm)	Thermal Conductivity (λ, W/mK)	Density (kg/m^3)	Area (m^2)	Heat Transfer Coefficient (U, W/m^{2}K)
Dolomite	600	2.2	2400	149.54	0.208
Existing plaster	20	0.87	1800		
Mineral wool	200	0.035	60		
Vapor barrier					
Plasterboard	12.5	0.21	680		
Interior decoration					

Table 2. Facade construction after retrofit in 2015: Type 2.

Material	Thickness (mm)	Thermal Conductivity (λ, W/mK)	Density (kg/m^3)	Area (m^2)	Heat Transfer Coefficient (U, W/m^{2}K)
Dolomite	600	2.2	2400	149.54	0.211
Existing plaster	20	0.87	1800		
Mineral wool	150	0.035	60		
Vapor barrier					
Plasterboard	12.5	0.21	680		
Interior decoration—painted wallpaper					

Table 3. Facade construction after retrofit in 2015: Type 3.

Material	Thickness (mm)	Thermal Conductivity (λ, W/mK)	Density (kg/m^3)	Area (m^2)	Heat Transfer Coefficient (U, W/m^{2}K)
Dolomite	450	2.2	2400	29.62	0.212
Existing plaster	20	0.87	1800		
Mineral wool	150	0.035	60		
Vapor barrier					
Plasterboard	12.5	0.21	680		
Interior decoration—painted wallpaper					

Table 4. Facade construction after retrofit in 2015: Type 4.

Material	Thickness (mm)	Thermal Conductivity (λ, W/mK)	Density (kg/m^3)	Area (m^2)	Heat Transfer Coefficient (U, W/m^{2}K)
Wood planks	25	0.2		22.78	0.215
Mineral wool	150	0.035	60		
Vapor barrier					
Plasterboard	12.5	0.21	680		
Interior decoration—painted wallpaper					

2.3. Energy Consumption

The building has a central heating system with a 40 kW firewood boiler integrated with a hot water storage tank. There are no mechanical ventilation or air conditioning units used in the building. The building has a natural ventilation system with air exchange through the building envelope. Room temperature can be regulated based on the occupancy with radiator thermostats. Residents maintain the comfort temperature of +20 °C in the inhabited rooms while reducing the temperature in rooms that are not occupied. The north-east side of the ground floor is occupied all year; the rest of the building is inhabited only on weekends, holidays, and during the summer.

3. Research Methodology

3.1. Construction Material Analysis

Dolomite stones used in the building have different structural patterns (see Figure 1). The study on lithological morphological types of dolomite historically used for the construction of stone buildings in Latvia predominantly is mechanically resistant marble-like dolomite [45]. Dolomite samples from the building were obtained and tested in the laboratory of the Riga Technical University to determine their main properties—density, specific heat capacity, thermal conductivity, total porosity, capillary saturation, water vapor resistance factor, water uptake coefficient, and moisture storage. These values were further used as input data to characterize the material's properties in the simulation program DELPHIN [46].

Laboratory data were determined through a series of tests. Depending on the test, three to twenty-two specimens were prepared (cut, pre-conditioned) to obtain information on the properties' variance and minimize irregularity effects. In addition to the standard test methods [47–51], other methods [52,53] were also used. The test methods are summarized in Table 5.

Table 5. Test methods for the properties of the dolomite stone.

Name of the Material Property	Name of the Corresponding Experiment
Bulk density	Via dimensions and weight of the sample [41]
Open porosity	Calculated from density [48,52]
Thermal conductivity	Heat flux measurement (plate apparatus) [52]
Heat storage capacity	Calorimeter experiment [52]
Dry-cup vapor diffusion	μ dry-cup measurement [49]
Wet-cup vapor diffusion	μ wet-cup measurement [49]
Water uptake coefficient	Water uptake experiment [51]
Capillary saturation moisture content	The final value of the water uptake experiment [52]
Sorption moisture content	Exicator/desiccator [52]

3.2. Energy Consumption Simulation

The dynamic simulation tool TRNSYS Type 56 (2016) [54] was used to calculate the building's energy balance. For the simulation, the building was divided into zones A1—basement and A2—above-ground floors (See Figure 5). The primary input data are shown in Table 6.

Table 6. Main input data about the case study building.

	Orientation				Heat Transfer Coefficient U, W/m^{2}K	
	North	**East**	**West**	**South**	**Before Renovation**	**After Renovation**
Facade walls (m^2)						
Basement	9.14	18.9	-	5.08	2.259	2.259
Basement in contact with soil	-	15.12	34.02	4.06		
Ground floor	32.4	56.7	56.7	32.4	2.147	0.208
1st floor (3rd type)	17.28	-	-	17.28	2.515	0.211
1st floor (4th type)	4.32	8.47	8.47	4.32	-	0.215
Windows (m^2)						
Basement	-	1.68	-	1.12	2.83	2.83
Ground floor	1.68	8.4	8.4	3.36	2.83	1.26
1st floor (3rd type)	2.47	-	-	2.47	2.83	1.26
1st floor (4th type)	-	1.24	1.57	-	-	1.26
Doors (m^2)						
Basement	1.44	-	-	-	2.83	2.83
Ground floor	1.98	1.98	2.86	-	2.83	2.83
Floor area on the ground	108.11				2.395	2.395
Basement ceiling	96.01				0.668	0.34
Roof area	-	141.4	141.4	-	1.087	0.110

Three scenarios were simulated:

- The baseline: the building before both renovations;
- The building with internal insulation on the walls of the ground and 1st floor;

- The building with additional energy-saving measures (insulation of basement ceiling and roof, replacement of windows).

The simulations for all scenarios were based on the following assumptions: (1) climatic data of Latvia defined by the software used as an input file in the TRNSYS were used; (2) indoor temperature +20 °C in zone A2 when the building is in use, e.g., workdays in the morning (6 am to 8 am) and in the evening (4 pm to 11 pm) and full days on weekends, and +18 °C the rest of the time; (3) indoor relative humidity 50%; (4) infiltration 0.05 h^{-1}, with additional natural ventilation during the opening of windows for zone A2—0.5 h^{-1}; (5) heat gains are based on values defined in EN ISO 13790:2008 [55], all heat gains are scheduled.

3.3. In Situ Measurements

In December 2017, temperature, relative humidity, volumetric water content, and heat flux sensors were installed within the external walls on the north-east facade. One set of sensors was installed in the living room wall, and the other in the bathroom wall (see Figure 6b). Both walls were retrofitted in 2015. Additionally, the pyranometer Campbell CMP3 060271 with sensitivity 11.72 × 10^{-6} V/Wm^{-2} was installed on the north-east facade. Figure 6 shows the sensors' setup and their connections to the data loggers used in the setup. The setup of sensors is the same for the living room and bathroom, except for the solar radiation sensor. One solar radiation sensor was installed 5 m from the ground level. Indoor temperature measurements were performed by twisted pair T-type thermocouples—Labfacility XE-2342. Temperature sensor t1 measures the temperature between the dolomite wall and the insulation layer, and t2 measures the temperature between the insulation layer and the vapor barrier (see Figure 6a). These sensors were installed at the 1.8 m height from the floor, corresponding to 4 m from the ground level. RH1-2 measures relative humidity at the same places as temperature sensors. Honeywell HIH-4000-002 measures RH had an accuracy of ±3.5%. Heat flow in walls was measured with Hukseflux heat flux sensors. Volumetric water content is measured using the time domain (TDR) reflectometer Campbell CR616, with an accuracy of ±2.5% of volumetric water content (VWC) and operational temperature from 0 to 70 °C. The CR616 has been installed 3.5 m from the ground level.

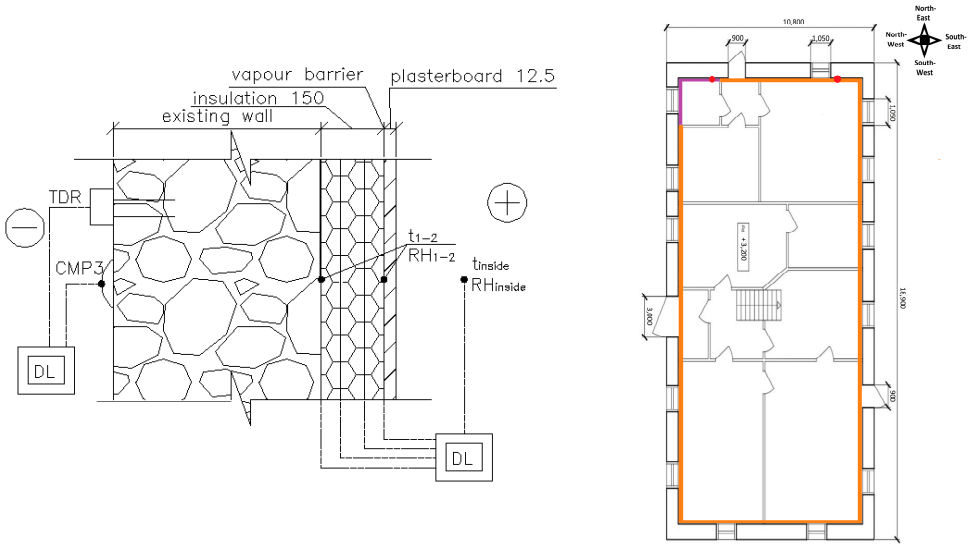

Figure 6. (**a**) Measurement setup (t—temperature; RH—relative humidity; CMP3—sun radiation, DL—data logger, TDR—volumetric water content.); (**b**) Measurement points: heat flow, temperature, and relative humidity sensors in the walls (the red dots).

Before installation, CR616 rods were shortened from the original 16 cm length to 10 cm length (due to restriction in drilling depth). Therefore, these sensors were recalibrated

afterward by using a sample dolomite stone from the case study building. During the calibration, the water-saturated dolomite sample mass and readings of the CR616 sensor were monitored. Based on that, a graph of water content vs. response time of the CR616 sensor specifically for dolomite stone was obtained (see Figure 7).

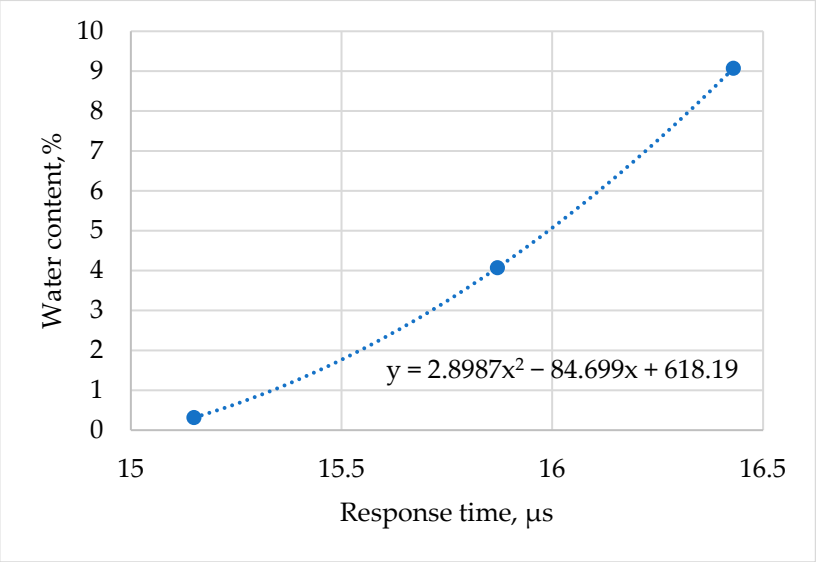

Figure 7. Calibration graph for TDR sensors.

Three data loggers were used for data logging: two Campbell Scientific CR1000 data loggers (one in the living room, one in the bathroom); one Campbell Scientific CR800 data logger (outside). A time step of 30 min for all measurements was taken. Data from data loggers were periodically collected.

3.4. Hygrothermal Calculations

The simulation tool DELPHIN 6.1. [46] and Glazer method was used to evaluate the hygrothermal behavior of the building's external walls with internal insulation. DELPHIN software is a simulation program for homogeneous layers to simulate heat and moisture mass transport and storage within the materials. The Glazer method is used for determining the conditions within the different layers of the wall at specific indoor and outdoor conditions. The simulation used climatic data entered by the software user. For indoor boundary conditions (temperature and relative humidity), data gained from in situ measurements were used. Weather data, such as outdoor temperature, relative humidity, wind speed and direction, hourly rain sum, and air pressure, were taken from weather station Skrīveri, located 20 km from the case study building, while sun radiation data were taken from the weather station Rīga—Universitāte located 100 km from the case study building. Both weather stations are operated by the state limited liability company "Latvian Environment, Geology and Meteorology Centre" (LEGMC) [56].

Material properties for plasterboard and mineral wool were imported from the DELPHIN material database. A vapor barrier was added as the resistance between material layers (sd = 2.3 m). Properties of dolomite were imported into the model as a new material file, using values obtained during the laboratory tests (Section 4.1). However, it should be noted that the load-bearing part of the walls is made from inhomogeneous natural materials. The results of laboratory tests also provide evidence of this during this research (Tables 5 and 6). For example, the density of the dolomite stone ranged from 1696.8 to 2949.5 kg/m^3, but the water vapor resistance factor from 26.67 to 77.83. Moreover, other research [56,57] about the properties of historical materials in Latvia showed a broad diversity in results.

4. Results

4.1. Construction Material Analysis

The results of the dolomite stone sample tests are summarized in Tables 7 and 8.

Table 7. Determined properties of the dolomite and corresponding test methods.

Name of the Material Property	Symbol (Unit)	Mean Value	Standard Deviation	Min Value	Max Value	Coefficient of Variance
Bulk density	ρ_b (kg/m^3)	2346.5	447.8	1696.8	2949.5	0.191
Open porosity	Θ_{por} (m^3/m^3)	0.1602	0.0224	0.1299	0.2008	0.140
Thermal conductivity	λ_{dry} (W/mK)	2.0478	0.0108	2.0362	2.0574	0.005
Heat storage capacity	c (J/kgK)	779.2842	5.1457	774.3023	784.5794	0.007
Dry-cup vapor diffusion	μ_{dry} (-)	44.14	29.18	26.67	77.83	0.661
Wet-cup vapour diffusion	μ_{wet} (-)	2113.88	943.36	1192.82	3078.06	0.446
Water uptake coefficient	A_w ($Kg/m^2\sqrt{s}$)	0.0599	0.0110	0.0477	0.0691	0.184
Capillary saturation moisture content	Θ_{cap} (m^3/m^3)	0.1079				

Table 8. Sorption moisture content.

RH (%)	t (°C)	Θ_l (φ) (m^3/m^3)			
		Mean Value	Standard Deviation	Min Value	Max Value
84.7	23	0.009524	0.000570	0.008907	0.01026
53.5	23	0.004830	0.000284	0.004553	0.00514
32.9	23	0.001787	0.003670	-9.982×10^{-5}	0.00926

4.2. Energy Consumption

The simulated annual heat consumption for space heating in the first scenario is 66.1 MWh/year or 194.4 kWh/m^2; in the second, it is 42.8 MWh/year or 125.8 kWh/m^2 (35% energy saving compared to the first scenario), and in the third, it is 18.3 MWh/year or 53.9 kWh/m^2 (72% energy saving compared to the first scenario).

The wood log consumption is not precisely registered and accounted for by the building residents because they directly cut part of the wood logs in the forest. Based on the data provided by the residents, around 30 m^3 (adjusted for empty spaces between individual firewood logs with a coefficient of 0.61) of two years of dried firewood has been used in the 2017/2018 heating season. By assuming that the moisture content of the firewood after two years of drying is 20% and the 40 kW burner's efficiency of η = 75%, the calculated annual energy consumption per heated area should be 87 kWh/m^2, which is higher than calculated in the third scenario (53.9 kWh/m^2). Various reasons can cause the difference, including:

- Poor quality of construction works;
- Inaccurate assumption of indoor temperature and relative humidity;
- An inaccurate pattern of heat gain schedule in the calculation model;
- Inaccurate climatic input data in the model;

- Inaccurate assumptions about the volume and moisture content of firewood;
- Inaccurate assumption of efficiency of the biomass boiler.

Other researchers [26,58–60] pointed out the issue of result diversity using different building simulation programs to simulate energy consumption or hygrothermal performance of historic buildings. Moreover, used software may need to capture the physical phenomena in historic buildings adequately. For example, heat flux measurements performed later in the case study building showed that the heat transfer coefficient of the living room wall is 0.21 W/m^{2}K (Section 4.3.2). It corresponds to the values entered into the model 0.208–0.2115 W/m^{2}K (see Table 6).

4.3. In Situ Measurement Results

The measurement period was from 13 December 2017 to 4 January 2019. However, due to failures in data logging equipment, gaps in collected data are present.

4.3.1. Measured Climatic Conditions

The monthly average outdoor temperature and relative humidity are presented in Figure 8. The most significant temperature shifts were observed during the winter months (December, January, and February), with February being the coldest month, e.g., the lowest registered temperature was −23.6 °C. The highest relative humidity was observed during late autumn and winter, falling over the spring months and increasing again during summer.

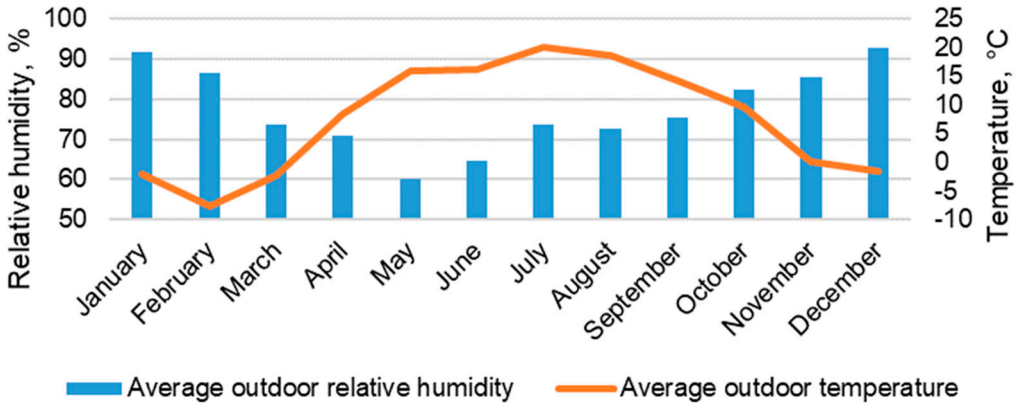

Figure 8. The monthly average outdoor relative humidity and temperature (data from the weather station "Skriveri").

The manual operation of the boiler causes fluctuations in the indoor air temperature. Monitoring results of the indoor temperature show that the residents try to maintain a constant room temperature during the day, letting it fall to +16 °C in the evening and then increasing the temperature before the night. Temperature increase from +16 to +22 °C takes around 2 to 3 h. During the winter months (December to March), the average indoor air temperature was +22 °C in the living room and +20.8 °C in the bathroom. The average indoor relative humidity was 35.7% in the living room and 40% in the bathroom. During spring months (April and May), the average temperature was +21.4 °C in the living room and +21.2 °C in the bathroom, and the average relative humidity was 47% in the living room and 50.4% in the bathroom. During the summer, relative humidity increased to 70% in the living room and over 80% in the bathroom. High relative humidity in the bathroom is expected as higher moisture loads are present in this room. During the monitored period, 2% of the time, relative humidity reached over 80%. After the relative humidity spike ends, it takes around 2–3 h for the relative humidity to drop from over 80% to under 70%.

4.3.2. Measured Conditions in the Wall

TDR measurement results show that water content mostly stays below 2% at both measurement points, and even after the rainfalls, when moisture content spikes appear, the wall does not reach saturation (see Figure 9).

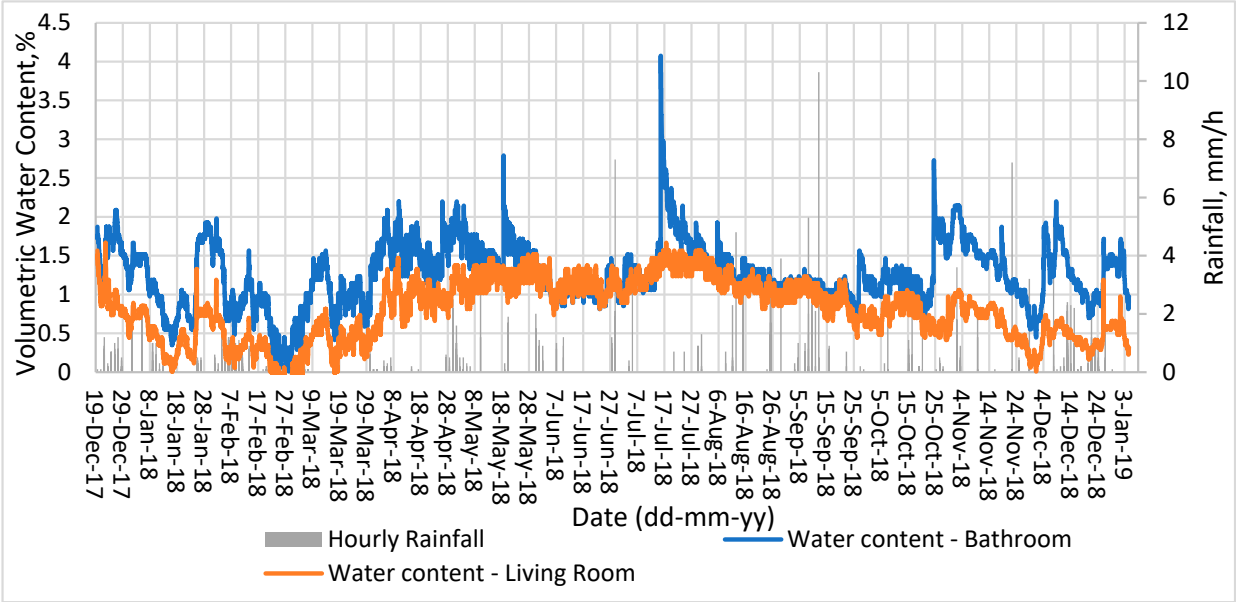

Figure 9. Results of water content measurements and rainfall (mm).

From the heat flux measurement and calculated indoor/outdoor temperature difference, a U-value of 0.21 W/(m^{2}K) for the living room wall and U = 0.19 W/(m^{2}K) for the bathroom wall was calculated.

4.4. Hygrothermal Calculation Results

Evaluation of the hygrothermal conditions with the Glazers method and 1D simulations in the DELPHIN 6.1 were performed. The eight months were chosen for the simulations to correspond to the available measurement data. For the Glazers method, average climatic conditions for Latvia were used (see Table 9).

Table 9. Average indoor and outdoor conditions for Latvia.

	Temperature, °C	Relative Humidity, %
Indoor	20	50
Outdoor	0	80

4.4.1. Measured and Simulated Conditions in the Wall

For wall type 1, the water vapor diffusion ratio of the cold and warm sides is 2.85, which is lower than the normative value (ratio > 5). Therefore, the saturated and partial pressure calculation for all planes of the type 1 wall was performed utilizing the Glazers method. For the calculations, the indoor temperature of 20 °C and outdoor temperature of 0 °C, outdoor humidity of 80%, and indoor humidity of 50% was used. Interstitial planes under the insulation material were found to be most prone to condensation (see Figure 10).

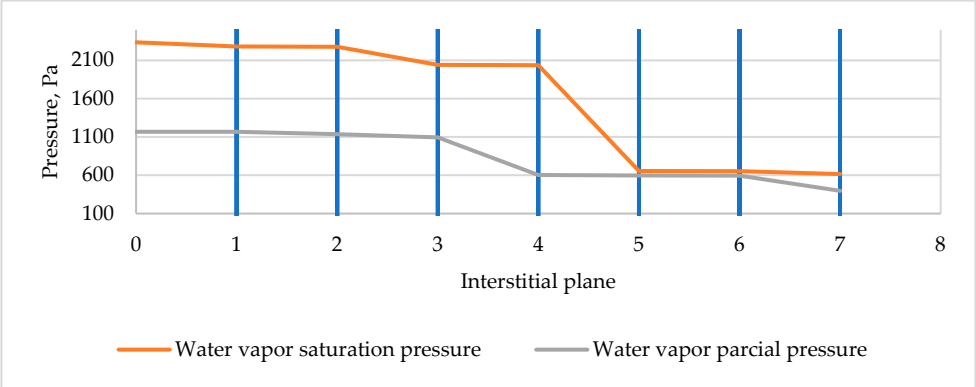

Figure 10. Partial and saturation pressures in interstitial planes for wall type1 (1. interior surface; 2. wallpaper/plasterboard; 3. vapor barrier/plasterboard; 4. mineral wool/vapor barrier; 5. plaster/mineral wool; 6. dolomite/plaster; 7. exterior wall surface).

Therefore, relative humidity calculations for interstitial planes on both sides of the vapor barrier and planes under the insulation material were performed for the range of outdoor temperatures (from +20 to −20 °C). The calculation results indicate the risk of interstitial condensation in the layer between wood planks and insulation (under the insulation) when the outdoor temperature drops below −5 °C. In the other high condensation-risk planes, there is no condensation risk within the given temperature range. (see Figure 11).

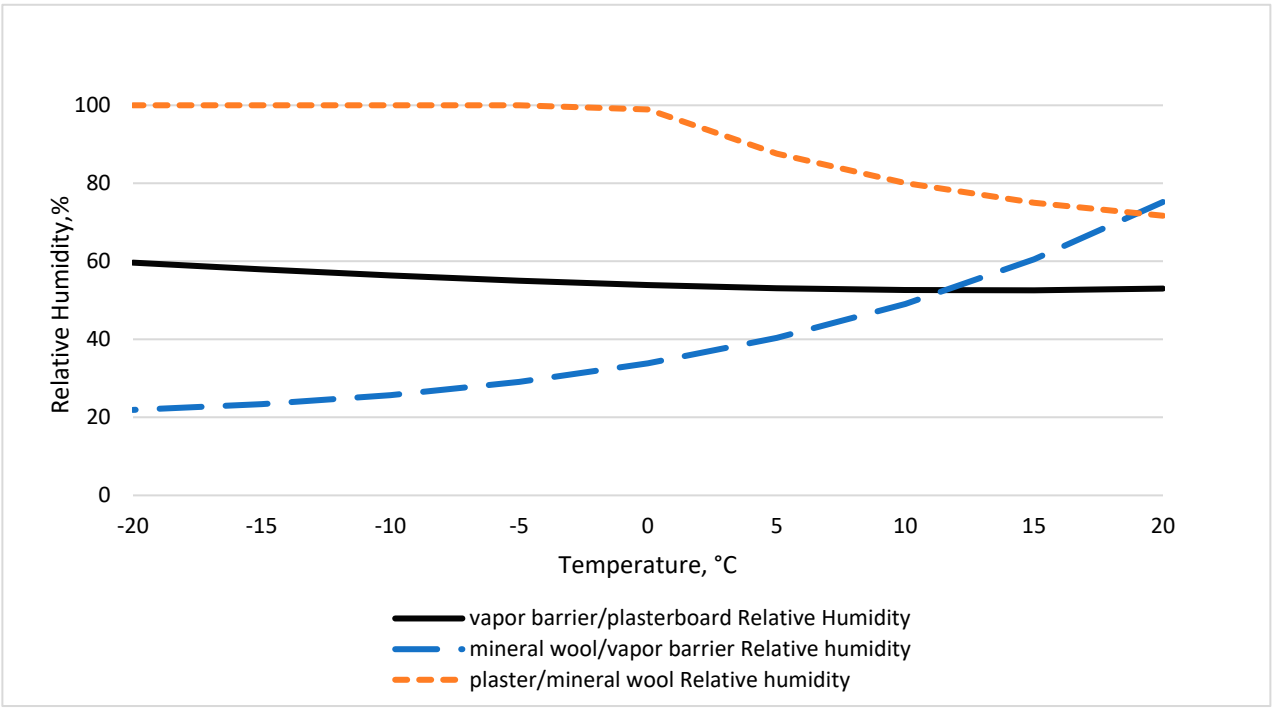

Figure 11. Calculated relative humidity at different interstitial planes for wall Type 1.

All three other wall types also did not reach the minimum normative warm/cold side ratio (type 2 = 2.85; type 3 = 3.78; type 4 = 1.74); therefore, the saturated and partial pressure calculation for all planes of all wall types was performed. As for wall type 1 and all the other wall types, the interstitial planes under the insulation material were found to be most prone to condensation. Therefore, the same relative humidity calculations for wall type 1 were performed for all the other wall types. The results for all the other wall types were very similar to those for wall type 1, with condensation risk under the insulation when the

temperature drops belove −5 °C and no condensation risk in other planes within the given temperature range.

4.4.2. Measured and Simulated Conditions in the Wall

The measured RH between the insulation layer and vapor barrier never exceeds 80%, mostly staying below 40% during winter and below 60% during the spring and summer. The exception was on 8 March 2018, when water leakage from the first-floor water supply system was detected. On that date, the RH between insulation and vapor barrier rapidly rises from 25% to 60% and then slowly decreases within the next two weeks (see Figure 12).

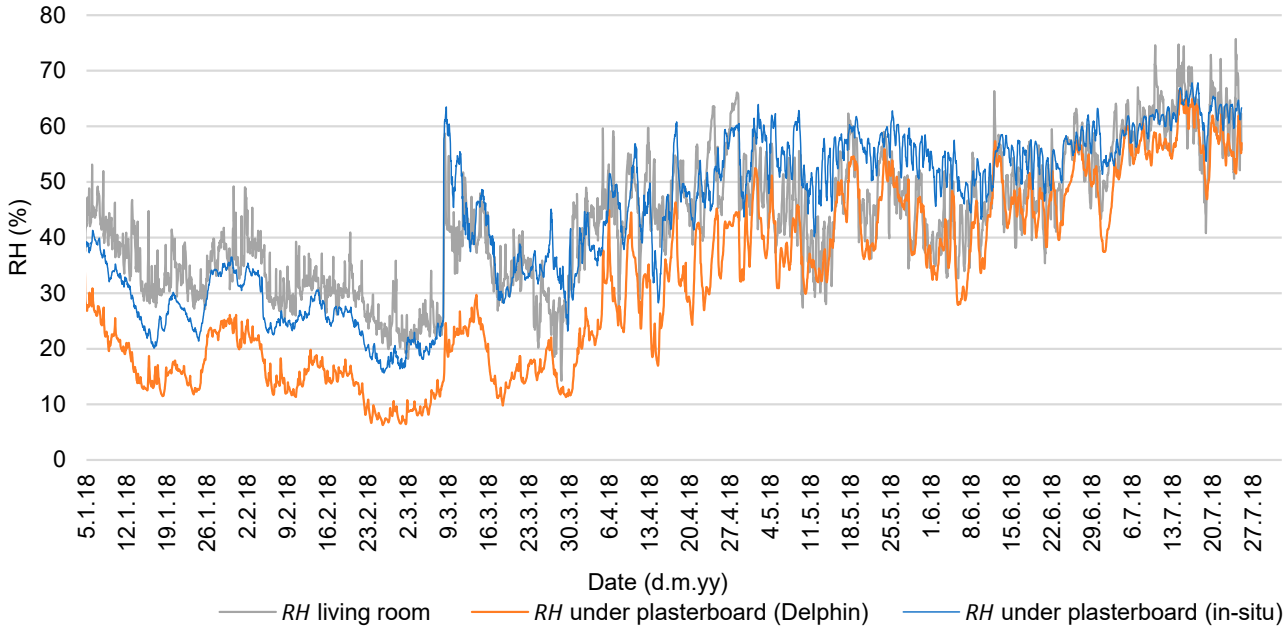

Figure 12. Relative humidity of the living room wall between the insulation and vapor barrier: measured RH (blue line), simulated RH (orange line), and indoor RH (grey line).

Simulated RH between the insulation and vapor barrier follows the trend of the indoor RH, although it is 5 to 10% lower than the level measured during the heating season (see Figure 12).

Simulated temperatures between the insulation and vapor barrier closely follow indoor temperature changes, with the difference in absolute values during winter. Differences between simulated and measured temperatures at the interface of the insulation and vapor barrier are most likely caused by the placement of room temperature sensors—off the wall and on the side of a closet (see Figure 6b). At that point, the temperature is higher than on the wall's surface. Moreover, measured temperatures are impacted more by fluctuations in the outside temperature. At the same time, simulated data follows room temperature, which in the simulation model was indicated as the climate data of the room (see Figure 13).

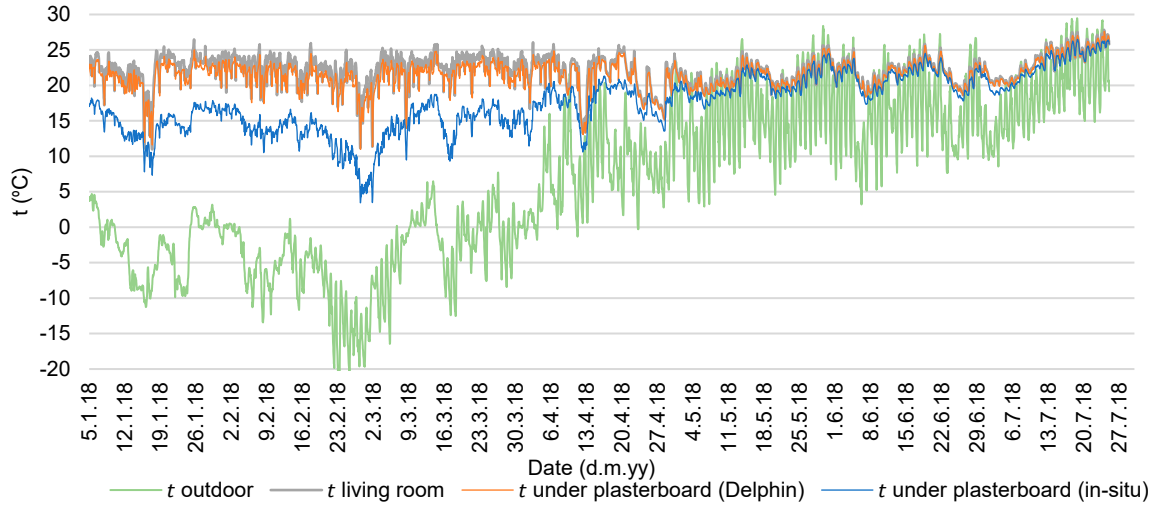

Figure 13. The temperature of the living room wall between the insulation and vapor barrier: measured T (blue line), simulated T (orange line), indoor T (grey line), and outdoor T (green line).

RH under the insulation mostly stays between 60 and 80%. Measured RH exceeded 90% in March during the water leakage incident when RH between the dolomite wall and insulation layer rapidly increased to 100% and then slowly dried out during the spring and summer (see Figure 14).

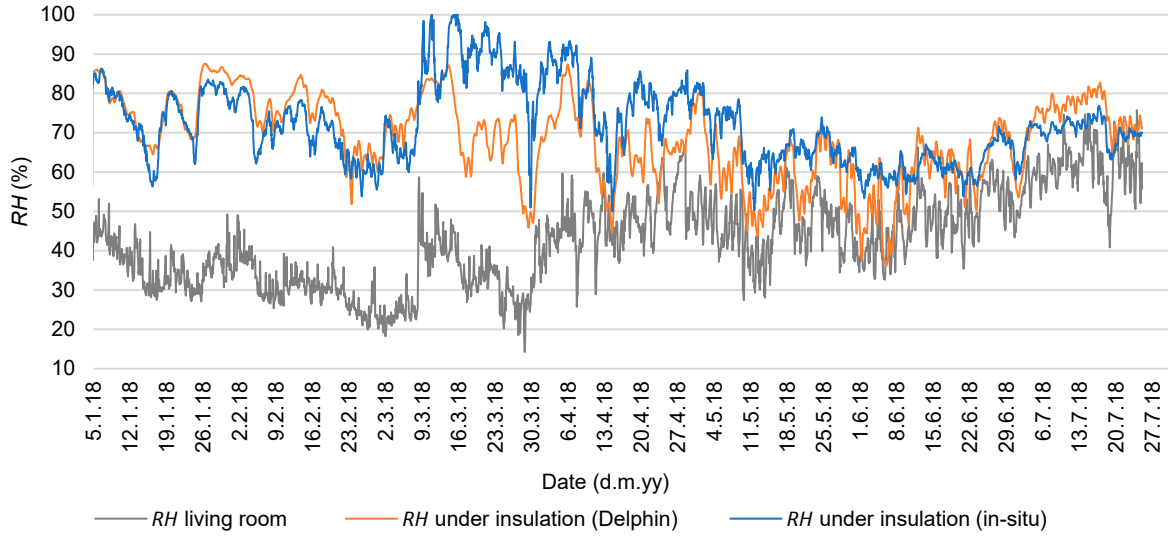

Figure 14. Relative humidity of the living room wall between dolomite and the insulation layers: measured RH (blue line), simulated RH (orange line), indoor RH (grey line), and outdoor RH (green line).

In the living room, the measured and simulated temperatures under the insulation follow a similar trend, but the simulated temperatures are around 1 degree lower than the measured. When the outside temperature drops below −5 °C, the temperature between the dolomite wall and insulation layer drops below 0 °C. However, there are no risks related to frost damage as the moisture content in the materials of the wall never reaches capillary saturation (see Figure 15).

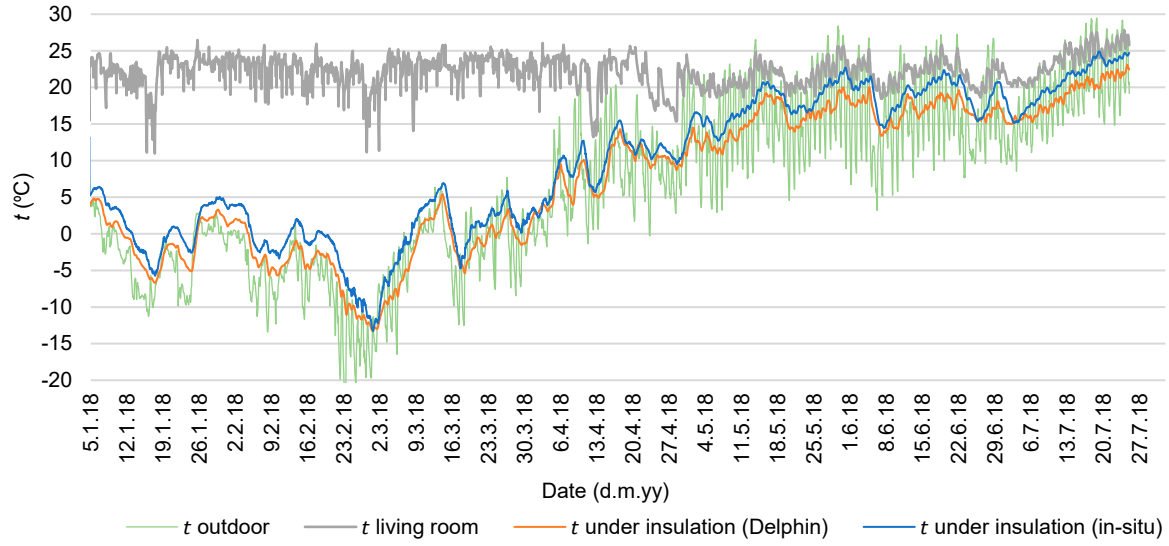

Figure 15. The temperature within the living room wall between dolomite and the insulation layers: measured T (blue line), simulated T (orange line), indoor T (grey line), and outdoor T (green line).

The bathroom RH between the insulation layer and vapor barrier never exceeds the critical level of 80%, mostly staying below 40% during the cold season and below 70% during the spring and summer (see Figure 16).

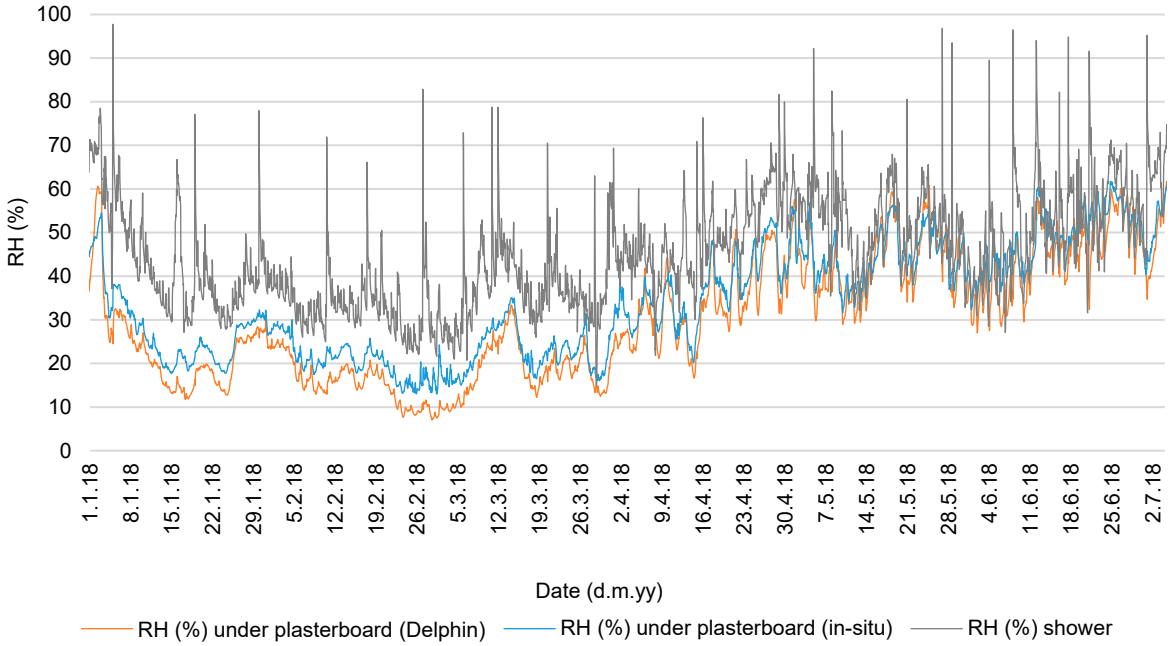

Figure 16. Relative humidity measurements of the bathroom wall between the insulation and vapor barrier: Measured RH (blue line), simulated RH (orange line), indoor bathroom RH (grey line).

Temperature between the insulation and vapor barrier in the bathroom shows similar data for measured and simulated data, with simulated data being slightly higher and closer to the measured indoor air temperature (see Figure 17).

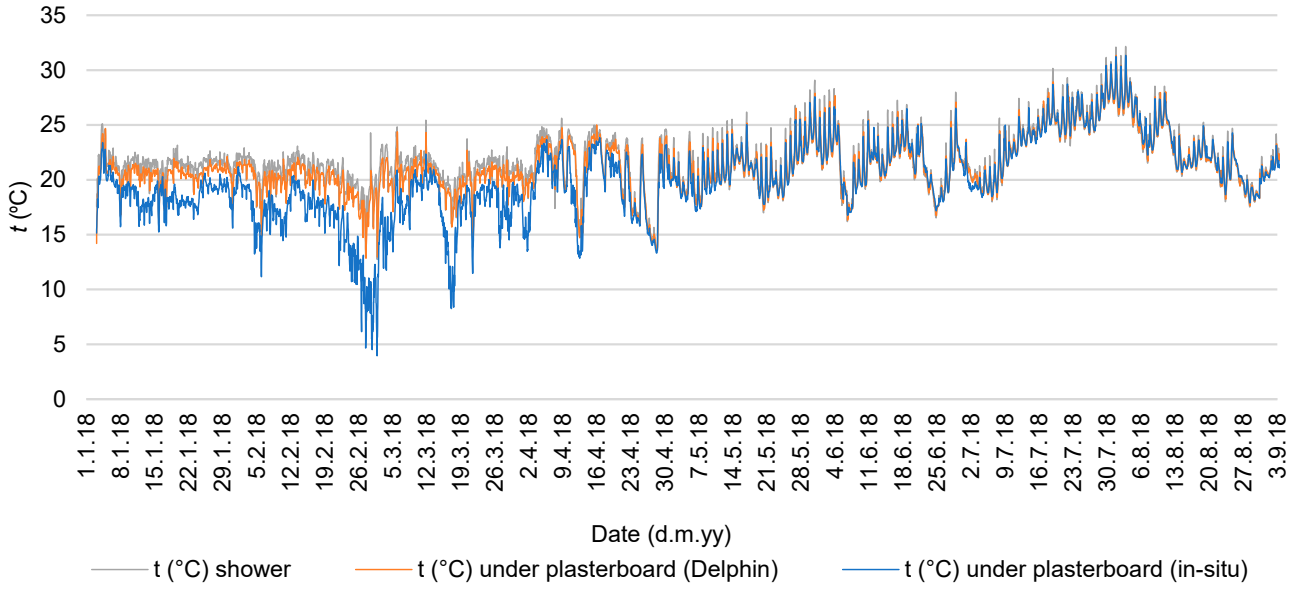

Figure 17. The temperature of the bathroom wall between the insulation and vapor barrier: measured T (blue line), simulated T (orange line), and indoor bathroom T (grey line).

The bathroom measured RH between dolomite and insulation mostly stays below 80% during autumn, winter, and spring and below 70% during summer. The simulated data for the same plane shows a higher RH of up to 90% (see Figure 18).

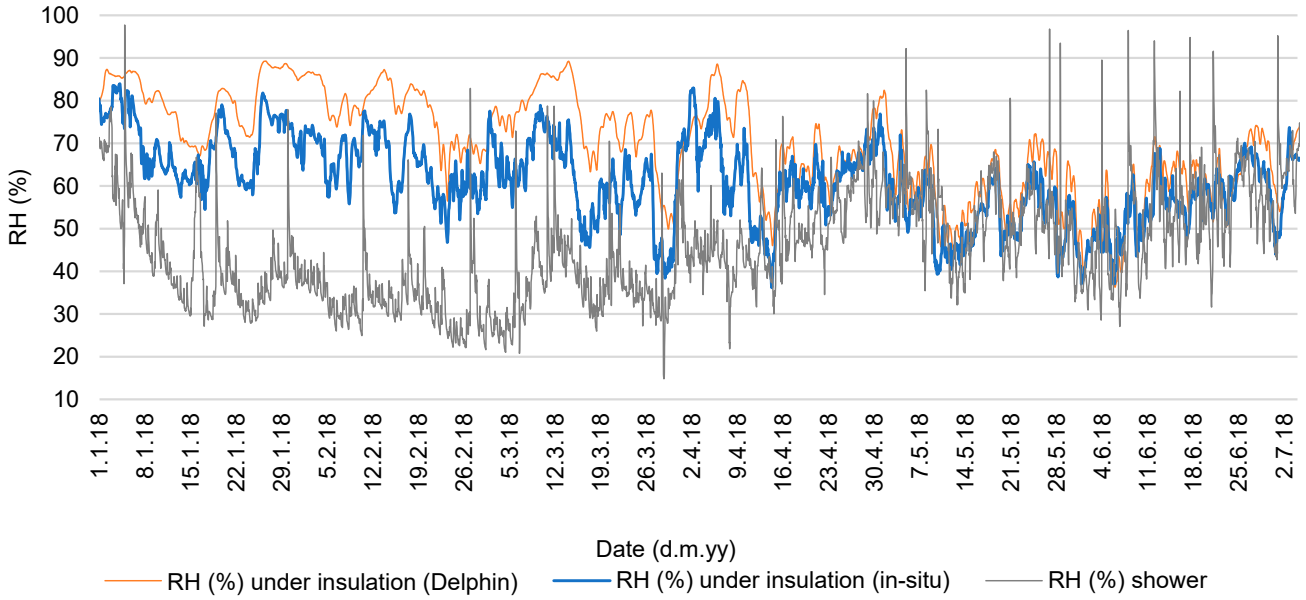

Figure 18. Relative humidity of the bathroom wall between dolomite and insulation layers: measured RH (blue line), simulated RH (orange line), indoor RH (grey line), and outdoor RH (green line).

Measured temperatures between dolomite and insulation follow outside temperatures during the heating season and are between outdoor and indoor temperatures outside the heating season (see Figure 19).

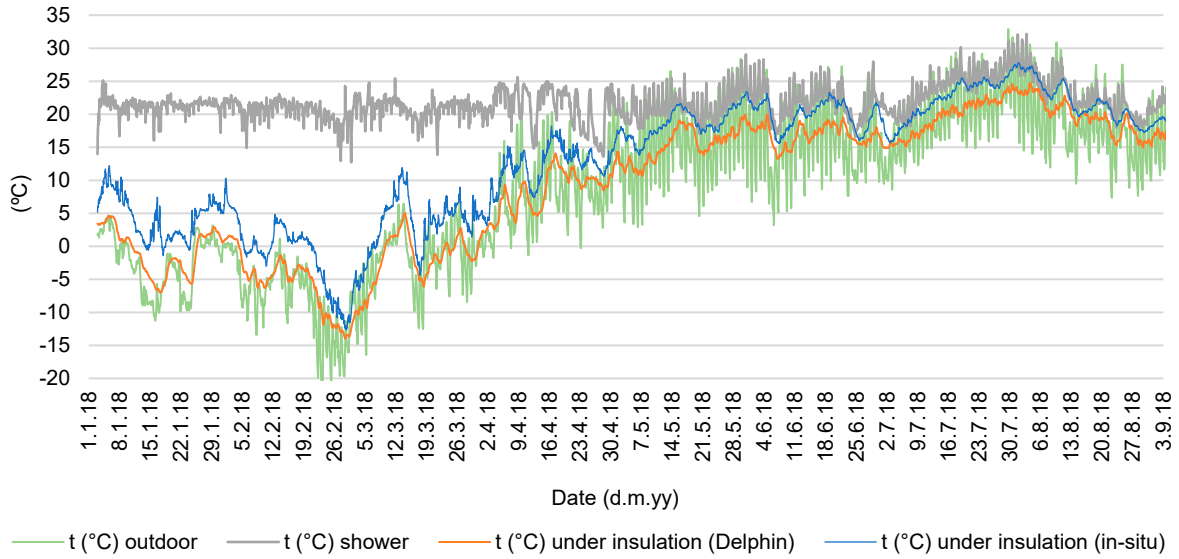

Figure 19. The temperature of the bathroom wall between dolomite and insulation layers: measured T (blue line), simulated T (orange line), indoor T (grey line), and outdoor T (green line).

4.4.3. Comparison of Experimental and Hygrothermal Simulation Results

The living room temperature correlation between dolomite and insulation (t under insulation) is strong (R^2 = 0.9789). However, the correlation between the insulation and vapor barrier is considerably lower (R^2 = 0.4003). The RH correlation is strong (R^2 = 0.9047) between the insulation and vapor barrier, and the correlation is weaker (R^2 = 0.4775) between dolomite and insulation (see Figure 20).

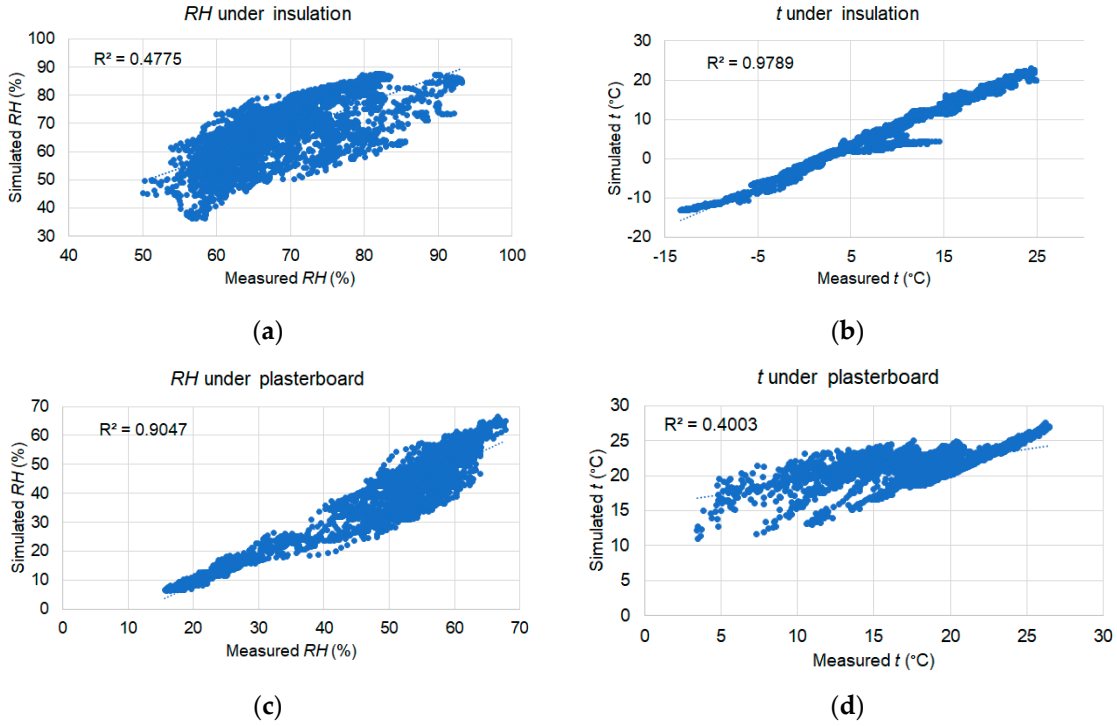

Figure 20. Correlation between simulated and measured RH and t in the living room wall: (**a**) RH between dolomite and insulation; (**b**) t between dolomite and insulation; (**c**) RH between the insulation and vapor barrier; (**d**) t between the insulation and vapor barrier.

The bathroom temperature correlation between dolomite and insulation (t under insulation) is strong (R^2 = 0.9778), and the insulation and vapor barrier correlation is also

strong (R^2 = 0.7876). The simulated and measured RH correlation between dolomite and insulation is moderate (R^2 = 0.633). In the case of RH between the insulation and vapor barrier, the correlation between measured and simulated data is strong (R^2 = 0.9694) (see Figure 21).

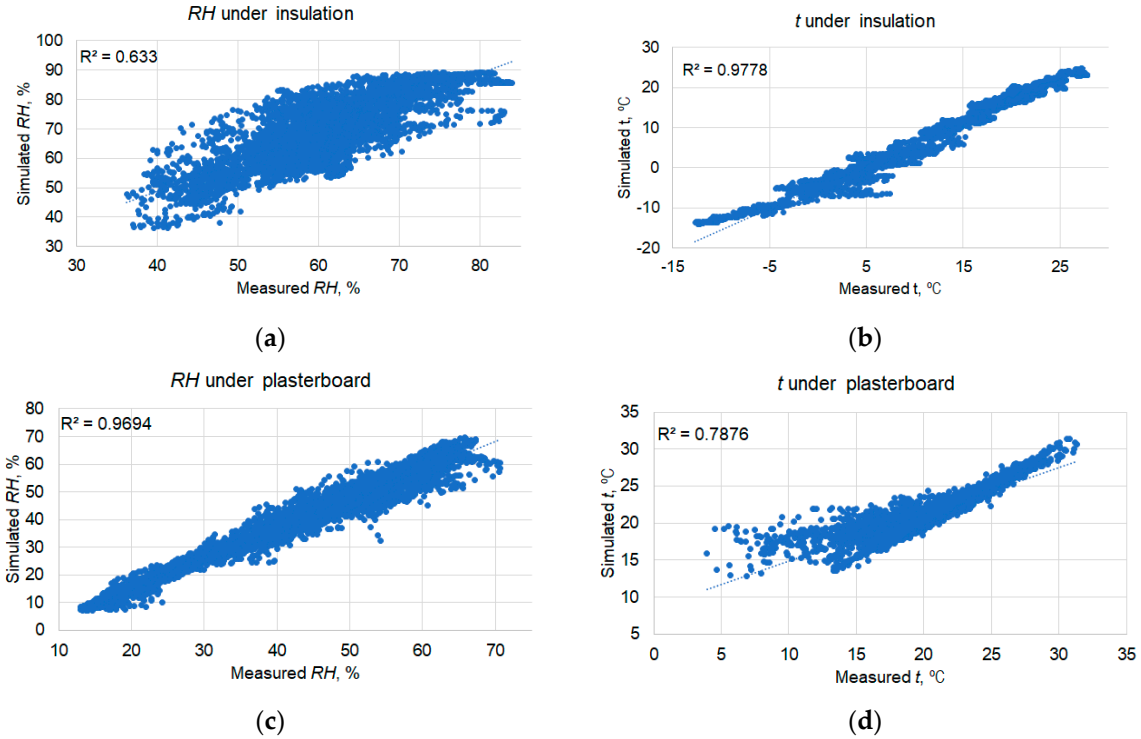

Figure 21. Correlation between simulated and measured RH and temperature in the bathroom wall: (**a**) RH between dolomite and insulation; (**b**) t between dolomite and insulation; (**c**) RH between the insulation and vapor barrier (**d**) t between the insulation and vapor barrier.

This correlation analysis does not include possible deviation of measurement accuracy, and three-week data following the water leakage accident were not used in the correlation analysis for the living room wall. Furthermore, outside temperatures and relative humidity data are taken from the weather station Skriveri, which is located 20 km away from the case study building.

The gap between the measured and simulated hygrothermal performance of internally insulated masonry walls was also seen in the previous study, where experimental results obtained in the controlled laboratory environment were compared to simulated results [28]. The research [61] showed that temperatures had a satisfactory correlation (R^2 in the range of 0.81 to 0.86), but walls insulated with mineral wool had the lowest correlation for measured and simulated RH (R^2 = 0.540). This corresponds to the research findings that the correlation for measured and simulated temperatures between masonry and insulation is strong but lower for relative humidity.

5. Discussions and Conclusions

This study aimed to answer two research questions. The first question was: what is the impact of internally insulated natural stone buildings on the hygrothermal behavior of walls in a cold climate? In situ measurements and hygrothermal simulations were carried out to evaluate the impact of internal insulation on the hygrothermal behavior of historic stone buildings in a cold climate. The assessment was performed for two occupied rooms located in the north-east facade. One of the rooms has a high indoor moisture load, while the other has an average moisture load. The results showed acceptable hygrothermal conditions within the wall. As the relative humidity between the insulation layer and vapor barrier and in the room stays relatively low (below 60%), excluding water

leakage accidents, the external wall does not indicate risks related to mold growth. Relative humidity reaches above critical 80% between the dolomite wall and insulation layer only for short periods. However, temperatures are lower than needed for spore germination (initial mold growth) at these moments and at this location. According to the literature review by Isaksson et al. [62], mold growth can occur at 80% high relative humidity if the temperature is at least 20 °C for porous materials. However, given that during the renovation in 2015, the tenants found mold on the bathroom wall, there is good potential for mold growth if appropriate conditions (high relative humidity and temperature) remain long enough as wall materials contain mold spores. In situ temperature measurements show that the outer part of the dolomite wall undergoes repeated freeze–thaw cycles. However, the risk of frost decay is minimal as the dolomite does not reach saturation [63]. Results of hygrothermal modeling validate the reliability of the prediction of hygrothermal conditions and risks of mold growth and frost damage in internally insulated historic buildings.

The second research question was: what energy savings can be reached by internal insulation of natural stone buildings in a cold climate? The simulated annual heat consumption for space heating in the baseline scenario can be reduced by 35% if internal insulation is applied on the ground and first-floor walls. If the significant energy efficiency renovation (internal wall insulation, basement ceiling, roof insulation, replacement of windows) is carried out, baseline energy consumption can be reduced by 72%. Actual energy consumption is calculated based on the data provided by the residents who count for primary energy resources—firewood which is partly supplied directly from the forest and dried on site. If the wood log consumption is converted into final energy, the annual energy consumption per heated area should be 87 kWh/m^2. Energy savings are 17% less than calculated in the simulation model. Several reasons could cause this difference, such as uncertainty of the quality of construction works and remaining thermal bridges, input data of the model, including factors related to occupancy frequency (heat gains, room temperature, and ventilation frequency). Simulation results are sensitive to the quality of input data, such as room temperature, relative humidity, ventilation, and material properties. In historic buildings, there is a lack of detailed information on wall cavities, ratio and typology of stones and mortar, construction defects, and specific properties of materials. On the other hand, the uncertainty of actual primary energy consumption, including the amount and quality of firewood efficiency of energy transformation technologies, significantly impacts the final energy consumption values.

Author Contributions: Conceptualization, A.B.; Methodology, A.K.; Software, E.B.; Investigation, R.F. All authors have read and agreed to the published version of the manuscript.

Funding: This study is carried out in the scope of EU financed project "RIBuild—Robust Internal Thermal Insulation of Historic Buildings" (637268-RIBuild-H2020-EE-03-2014).

Data Availability Statement: Zenodo "RIBuild: Measurements at case buildings with internal insulation (DK, LV, IT)", DOI: 10.5281/zenodo.3890099.

Conflicts of Interest: The authors declare no conflict of interest.

References

1. Directive (EU) 2018/844 of the European Parliament and the Council of 30 May 2018 amending Directive 2010/31/EU on the energy performance of buildings and Directive 2012/27/EU on energy efficiency. *Off. J. Eur. Union* **2018**, *156*, 75–91.
2. European Commission. *A Clean Planet for All—A European Strategic Long-Term Vision for a Prosperous, Modern, Competitive and Climate Neutral Economy, COM*; European Commission: Brussels, Belgium, 2018.
3. Factsheet: Energy Performance in Buildings Directive. European Commission, January 2019. Available online: https://ec.europa.eu/energy/content/factsheet-energy-performance-buildings-directive_en?redir=1 (accessed on 2 December 2022).
4. Gynther, L.; Lapillonne, B.; Pollier, K. Energy Efficiency Trends and Policies in the Household and Tertiary Sectors—An Analysis Based on the ODYSSEE and MURE Databases. Available online: http://www.odyssee-mure.eu/publications/br/energy-efficiency-trends-policies-buildings.pdf (accessed on 2 December 2022).
5. Communication from the Commission: The European Green Deal. Brussels 11.12.2019. Available online: https://eur-lex.europa.eu/legal-content/EN/TXT/?qid=1576150542719&uri=COM%3A2019%3A640%3AFIN#footnote6 (accessed on 2 December 2022).

6. La Fleur, L.; Rodin, P.; Moshfegh, B. Energy renovation versus demolition and construction of a new building—A comparative analysis of a Swedish multi-family building. *Energies* **2019**, *12*, 2218. [CrossRef]
7. Gaspar, P.L.; Santos, A.L. Embodied energy on refurbishment vs. demolition: A southern Europe case study. *Energy Build.* **2015**, *87*, 386–394. [CrossRef]
8. Berg, F.; Fuglseth, M. Life cycle assessment and historic buildings: Energy-efficiency refurbishment versus new construction in Norway. *Archit. Conserv.* **2018**, *24*, 152–167. [CrossRef]
9. Economidou, M.; Laustsen, J.; Ruyssevelt, P.; Staniaszek, D. Europe's Buildings under the Microscope. Available online: http://bpie.eu/publication/europes-buildings-under-the-microscope/ (accessed on 2 December 2022).
10. European Commission, An EU Strategy on Heating and Cooling, COM. 2016. Available online: https://eur-lex.europa.eu/LexUriServ/LexUriServ.do?uri=COM:2016:0051:FIN:EN:PDF (accessed on 2 December 2022).
11. Mazzarella, L. Energy retrofit of historic and existing buildings. The legislative and regulatory point of view. *Energy Build.* **2015**, *95*, 23–31. [CrossRef]
12. Murgul, V.; Pukhkal, V. Saving the Architectural Appearance of the Historical Buildings due to Heat Insulation of their External Walls. *Procedia Eng.* **2015**, *117*, 891–899. [CrossRef]
13. Claude, S.; Ginestet, S.; Bonhomme, M.; Escadeillas, G.; Taylor, J.; Marincioni, V.; Korolija, I.; Altamirano, H. Evaluating retrofit options in a historical city center: Relevance of bio-based insulation and the need to consider complex urban form in decision-making. *Energy Build.* **2019**, *182*, 196–204. [CrossRef]
14. Johansson, P.B.; Adl-Zarrabi, A.S. Kalagasidis, Evaluation of 5 years' performance of VIPs in a retrofitted building façade. *Energy Build.* **2016**, *130*, 488–494. [CrossRef]
15. Blumberga, A.; Kašs, K.; Kamendere, E. A review on Latvian historical building stock with heavy walls. *Energy Procedia* **2016**, *95*, 17–21. [CrossRef]
16. Ozel, M. Thermal performance and the optimum insulation thickness of building walls with different structure materials. *Appl. Therm. Eng.* **2011**, *31*, 3854–3863. [CrossRef]
17. Salvalai, G.; Sesana, M.M.; Iannaccone, G. Deep renovation of multi-story multi-owner existing residential buildings: A pilot case study in Italy. *Energy Build.* **2017**, *148*, 23–36. [CrossRef]
18. Pasichnyi, O.; Levin, F.; Shahrokni, H.; Wallin, J.; Kordas, O. Data-driven strategic planning of building energy retrofitting: The case of Stockholm. *J. Clean. Prod.* **2019**, *233*, 546–560. [CrossRef]
19. Belaïd, F.; Ranjbar, Z.; Massié, C. Exploring the cost-effectiveness of energy efficiency implementation measures in the residential sector. *Energy Policy* **2021**, *150*, 112112. [CrossRef]
20. van den Brom, P.; Meijer, A.; Visscher, H. Actual energy saving effects of thermal renovations in dwellings—Longitudinal data analysis including building and occupant characteristics. *Energy Build.* **2019**, *182*, 251–263. [CrossRef]
21. Cholewa, T.; Balaras, C.A.; Nižetić, S.; Siuta-Olcha, A. On calculated and actual energy savings from thermal building renovations—Long term field evaluation of multifamily buildings. *Energy Build.* **2020**, *223*, 110–145. [CrossRef]
22. Walker, R.; Pavía, S. Thermal performance of a selection of insulation materials suitable for historic buildings. *Build. Environ.* **2015**, *94*, 155–165. [CrossRef]
23. Odgaard, T.; Bjarløv, S.P.; Rode, C. Interior insulation—Characterisation of the historic, solid masonry building segment and analysis of the heat saving potential by 1d, 2d, and 3d simulation. *Energy Build.* **2018**, *162*, 1–11. [CrossRef]
24. De Mets, T.; Tilmans, A.; Loncour, X. Hygrothermal assessment of internal insulation systems of brick walls through numerical simulation and full-scale laboratory testing. *Energy Procedia* **2017**, *132*, 753–758. [CrossRef]
25. Vereecken, E.; Van Gelder, L.; Janssen, H.; Roels, S. Interior insulation for wall retrofitting—A probabilistic analysis of energy savings and hygrothermal risks. *Energy Build* **2015**, *89*, 231–244. [CrossRef]
26. Webb, A.L. Energy retrofits in historic and traditional buildings: A review of problems and methods, Renewable and Sustainable. *Energy Rev.* **2017**, *77*, 748–759.
27. Vereecken, E.; Roels, S. A comparison of the hygric performance of interior insulation systems: A hot box–cold box experiment. *Energy Build.* **2014**, *80*, 37–44. [CrossRef]
28. van Aarle, M.; Schellen, H.; van Schijndel, J. Hygro Thermal Simulation to Predict the Risk of Frost Damage in Masonry; Effects of Climate Change. *Energy Procedia* **2015**, *78*, 2536–2541. [CrossRef]
29. Bjarløv, S.P.; Finken, G.R.; Odgaard, T. Retrofit with interior insulation on solid masonry walls in cool temperate climates—An evaluation of the influence of interior insulation materials on moisture condition in the building envelope. *Energy Procedia* **2015**, *78*, 1461–1466. [CrossRef]
30. Zhao, J.; Meissner, F. Experimental investigation of moisture properties of historic building material with hydrophobization treatment. *Energy Procedia* **2017**, *132*, 261–266. [CrossRef]
31. Harrestrup, M.; Svendsen, S. Full-scale test of an old heritage multi-story building undergoing energy retrofitting with focus on internal insulation and moisture. *Build. Environ.* **2015**, *85*, 123–133. [CrossRef]
32. Bottino-Leone, D.; Larcher, M.; Herrera-Avellanosa, D.; Haas, F.; Troi, A. Evaluation of natural-based internal insulation systems in historic buildings through a holistic approach. *Energy* **2019**, *181*, 521–531. [CrossRef]
33. Tijskens, A.; Janssen, H.; Roels, S. A simplified dynamic zone model for a probabilistic assessment of hygrothermal risks in building components hygrothermal risks in building components. *Energy Procedia* **2017**, *132*, 717–722. [CrossRef]

34. Cuce, E.; Cuce, P.M. The impact of internal aerogel retrofitting on the thermal bridges of residential buildings: An experimental and statistical research. *Energy Build.* **2016**, *116*, 449–454. [CrossRef]
35. Cueto, N.D.; Benavente, J.; Martínez-Martínez, M.A. García-del-Cura, Rock fabric, pore geometry and mineralogy effects on water transport in fractured dolostones. *Eng. Geol.* **2009**, *107*, 1–15. [CrossRef]
36. Vázquez, P.; Alonso, F.J.; Carrizo, L.; Molina, E.; Cultrone, G.; Blanco, M.; Zamora, I. Evaluation of the petrophysical properties of sedimentary building stones intostablish quality criteria. *Constr. Build. Mater.* **2013**, *41*, 868–878. [CrossRef]
37. Lucchi, E. Thermal transmittance of historical stone masonries: A comparison among standard, calculated and measured data. *Energy Build.* **2017**, *151*, 393–405. [CrossRef]
38. Varas-Muriel, M.J.; Pérez-Monserrat, E.M.; Vázquez-Calvo, C.; Fort, R. Effect of conservation treatments on heritage stone. CCharacterizationof decay processes in a case study. *Constr. Build. Mater.* **2015**, *95*, 611–622. [CrossRef]
39. Benavente, D.; Martínez-Martínez, J.; Cueto, N.; García-del-Cura, M.A. Salt weathering in dual-porosity building dolostones. *Eng. Geol.* **2007**, *94*, 215–226. [CrossRef]
40. Toman, J.; Vimmrova, A.; Cerny, R. Long-term on-site assessment of the hygrothermal performance of interior thermal insulation system without a watevaporur barrier. *Energy Build* **2009**, *41*, 51–55. [CrossRef]
41. Klošeiko, P.; Arumagi, E.; Kalamees, T. Hygrothermal performance of internally insulated brick wall in a cold climate: A case study in a historic school building. *Build. Phys.* **2015**, *38*, 444–464. [CrossRef]
42. Wójcik, R.; Kosiński, P. On the rehabilitation of buildings with historical facades On the rehabilitation of buildings with historical façades. *Energy Procedia* **2017**, *132*, 927–932.
43. Hansen, T.K.; Bjarløv, S.P.; Peuhkuri, R.H.; Harrestrup, M. Long term in situ measurements of hygrothermal conditions at critical points in four cases of internally insulated historic solid masonry walls. *Energy Build.* **2018**, *172*, 235–248. [CrossRef]
44. Biseniece, E.; Žogla, G.; Kamenders, A.; Purviņš, R.; Kašs, K.; Vanga, R.; Blumberga, A. Thermal performance of internally insulated historic brick building in cold climate: A long term case study. *Energy Build.* **2017**, *152*, 577–586. [CrossRef]
45. Hodireva, V.; Sidraba, I.; Purviņš, E. Augšdevona dolomīta litoloģiski morfoloģiskie tipi Rīgas Kultūrvēsturiskajos piemineklos [Lithological morphological types of Upper Devonian dolomite in Riga Cultural Heritage Monuments]. *Mater. Sci. Appl. Chem.* **2010**, *22*, 105–113.
46. Simulation Tool DELPHIN. Available online: http://bauklimatik-dresden.de/delphin/index.php?aLa=en (accessed on 4 December 2022).
47. *EN 772-13:2000*; Methods of Test for Masonry Units. Determination of Net and Gross Dry Density of Masonry Units (Except for Natural Stone). BSI: London, UK, 2000.
48. *EN 772-3:1998*; Methods of Test for Masonry Units. Determination of Net Volume and Percentage of Voids of Clay Masonry Units by Hydrostatic Weighing. BSI: London, UK, 1998.
49. *EN ISO 12572:2001*; Hygrothermal Performance of Building Materials and Products—Determination of Water Vapour Transmission Properties. ISO: Geneva, Switzerland, 2001.
50. *EN ISO 12571:2013*; Hygrothermal Performance of Building Materials and Products—Determination of Hygroscopic Sorption Properties. ISO: Geneva, Switzerland, 2013.
51. *ISO 15148:2002*; Hygrothermal Performance of Building Materials and Products—Determination of Wa ter Absorption Coefficient by Partial Immersion. ISO: Geneva, Switzerland, 2002.
52. Project RIBuild. Available online: https://www.ribuild.eu/research-measurements/#10 (accessed on 4 December 2022).
53. Project RIBuild Deliverable D2.1 Report on the Material Properties. 2018. Available online: https://static1.squarespace.com/static/5e8c2889b5462512e400d1e2/t/5e9db81f43530a16d2f3fecf/1587394609561/RIBuild_D2.1_v1.0.pdf (accessed on 2 December 2022).
54. Simulation tool TRNSYS. Available online: http://www.trnsys.com (accessed on 4 December 2022).
55. *EN ISO 13790:2008*; Energy Performance of Buildings—Calculation of Energy Use for Space Heating and Cooling. ISO: Geneva, Switzerland, 2008.
56. State limited Liability Company Latvian Environment, Geology and Meteorology Centre. Available online: https://meteo.lv/meteorologija-datu-meklesana/?nid=461 (accessed on 2 December 2022).
57. Purviņš, R.; Kamendere, E.; Blumberga, A. Laboratory investigation of Latvian historic brick and measurements of water movement in historic masonry walls. *Energy Procedia* **2017**, *113*, 327–332. [CrossRef]
58. Kamendere, E.; Grava, L.; Zvaigznitis, K.; Kamenders, A.; Blumberga, A. Properties of bricks and masonry of historical buildings as a background for safe renovation measures. *Energy Procedia* **2016**, *95*, 119–123. [CrossRef]
59. Robertu, F.; Oberegger, U.F.; Gasparella, A. Calibrating historic building energy models to hourly indoor air and surface temperatures: Methodology and case study. *Energy Build.* **2015**, *108*, 236–243. [CrossRef]
60. Coelho, G.B.A.; Silva, H.E.; Henriques, F.M.A. Calibrated hygrothermal simulation models for historical buildings. *Build. Environ.* **2018**, *142*, 439–450. [CrossRef]
61. Biseniece, E.; Freimanis, R.; Purviņš, R.; Graveslins, A.; Pumpurs, A.; Blumberga, A. Study of Hygrothermal Processes in External Walls with Internal Insulation. *Environ. Clim. Technol.* **2018**, *22*, 22–41. [CrossRef]

62. Isaksson, T.; Thelandersson, S.; Ekstrand-Tobin, A.; Johansson, P. Critical conditions for onset of mould growth under varying climate conditions. *Build. Environ.* **2010**, *45*, 1712–1721. [CrossRef]
63. Litti, G.; Khoshdel, S.; Audenaert, A.; Braet, J. Hygrothermal performance evaluation of traditional brick masonry in historic buildings. *Energy Build.* **2015**, *105*, 393–411. [CrossRef]